

Crystal structure and chemical composition of Li-, Fe-, and Mn-rich micas

MARIA FRANCA BRIGATTI,^{1,*} ANNIBALE MOTTANA,² DANIELE MALFERRARI,¹ AND GIANNANTONIO CIBIN²

¹Dipartimento di Scienze della Terra, Università di Modena e Reggio Emilia, Modena, Italy

²Dipartimento di Scienze Geologiche, Università degli Studi Roma Tre, Roma, Italy

ABSTRACT

The crystal chemistry of three Li-, Fe-, and Mn-rich trioctahedral micas has been characterized by single-crystal X-ray diffraction. The samples are from Hirukawa mine, Japan: $(\text{Si}_{3.43}\text{Al}_{0.57})(\text{Al}_{1.00}\text{Fe}_{0.38}\text{Mg}_{0.01}\text{Mn}_{0.17}\text{Li}_{1.44})(\text{Na}_{0.05}\text{K}_{0.95})\text{O}_{10}\text{F}_{1.88}(\text{OH})_{0.12}$; from Mokrusha mine, Russia: $(\text{Si}_{3.30}\text{Al}_{0.70})(\text{Al}_{1.00}\text{Fe}_{0.36}\text{Mg}_{0.01}\text{Mn}_{0.31}\text{Li}_{1.32})(\text{Ca}_{0.01}\text{Na}_{0.04}\text{K}_{0.94})\text{O}_{10}\text{F}_{1.91}(\text{OH})_{0.09}$; and from Sawtooth Mountains, Boise County, Idaho, U.S.A.: $(\text{Si}_{3.11}\text{Al}_{0.89})(\text{Al}_{0.91}\text{Ti}_{0.02}\text{Fe}_{0.46}\text{Mg}_{0.03}\text{Mn}_{0.52}\text{Li}_{1.06})(\text{Na}_{0.05}\text{K}_{0.92}\text{Rb}_{0.02})\text{O}_{10}\text{F}_{1.89}(\text{OH})_{0.11}$. Our crystals belong to the *1M* polytype with layer symmetry *C121(1)* and show M1 and M3 sites much larger in size than M2. Mean electron-count (m.e.c.) values are more variable for the M1 and M3 sites than for M2. With the exception of the sample from Sawtooth Mountains, all tetrahedral mean bond lengths appear to be smaller for T1 than for T11 site. When compared to the Li- and Fe-rich series, crystals show similar crystal-chemical trends, thus suggesting that the layer structure is affected in a similar way by Fe and Mn cations.

Keywords: Masutomilite, polyolithionite, siderophyllite, pegmatite, crystal structure, crystal chemistry

INTRODUCTION

Li-, Fe-, and Mn-rich micas, uncommon in natural environments, are generally characterized by chemical data (Harada et al. 1976; Němec 1983a; Eggleton and Ashley 1989; Menzies and Boggs 1993; Abdalla et al. 1996; Förster et al. 2005). Crystal-structure data are limited or missing. The crystal-structure refinements of holotype masutomilite (Mizota et al. 1986) and norrishite (Tyrna and Guggenheim 1991) represent two relevant exceptions.

Norrishite ($\text{KLiMn}_2^3+\text{Si}_4\text{O}_{12}$) is known from one locality (Eggleton and Ashley 1989). It is a trioctahedral oxy-mica where the occurrence of Mn^{3+} in the octahedral sheet requires the complete deprotonation of the anionic site to match charge-balance constraints (Tyrna and Guggenheim 1991).

Masutomilite ($\text{KLiAlMn}^{2+}\text{AlSi}_3\text{O}_{10}\text{F}_2$; $0.5 \leq \text{Mn} \leq 1.0$; $3.0 \leq \text{Si} \leq 3.5$; $1.0 \leq \text{Li} \leq 1.5$; $0.5 \leq {}^{19}\text{Al} \leq 1.0$) is rare but not as unusual as norrishite (Harada et al. 1976; Němec 1983a, 1983b; Mizota et al. 1986). Unlike in norrishite, manganese is divalent and occurs with Fe^{2+} and Fe^{3+} . This trioctahedral mica shows octahedral ordering that produces a lowering of layer symmetry from the *C2/m* space group to *C2* (Mizota et al. 1986), like in most Li- and Fe-rich micas (cf. Brigatti and Guggenheim 2002 for review of the crystal structure and chemistry of Li-rich micas). More precisely, referring to diperic groups (Dornberger-Schiff et al. 1982), the layer symmetry lowers from *C12/m1(1)* to *C121(1)*, as the result of a different cation ordering in the *cis* octahedral

sites: trivalent cations (mainly Al^{3+}) are ordered at one *cis* site, whereas Li and Mn occupy the two remaining positions (i.e., the other *cis* site and the *trans* site).

Structural data are available for Li- and Fe-rich micas-*1M* (e.g., Guggenheim and Bailey 1977; Guggenheim 1981; Backhaus 1983; Brigatti et al. 2000). In contrast, no structural data are available for Li-rich micas with Fe and Mn as significant octahedral cations. This paper provides crystal chemical and structural data for three Li-rich micas-*1M* containing variable, but significant amounts of octahedral Mn and Fe. The aim of this investigation is to clarify the mechanisms of Li and Mn incorporation into the mica layer and to identify the ordering pattern for the octahedral (and possibly tetrahedral) sites.

MATERIALS AND METHODS

Samples

The studied samples are from three well-known localities where mica samples may crystallize as large blades at low pressure and medium temperature in a pegmatite rich in Li and Fe + Mn and in the presence of supercritical vapor, mainly F (Černý et al. 1985, 1986). At Hirukawa mine (Ena county, Gifu prefecture, Chubu region, Japan, labeled “Hirukawa”) the host rock is a granite with pegmatite pockets, containing crystals of smoky quartz, orthoclase, topaz, beryl, bertrandite, fluorite, cassiterite, zeolites, rare-earth (REE) minerals, and light yellow to pink micas trending in composition from zinnwaldite to masutomilite (Sueno et al. 2002). The sample studied here is very light pink and consists of several flakes in a star-like textural arrangement.

The Mokrusha mine (Yuzhakova village, Murzinka region, Russia, labeled “Mokrusha”) is at the center of a highly productive granitic pegmatite field (Alabashka field), where large gem-blue topaz, heliodor and aquamarine beryl, smoky quartz, and numerous rare mineral species occur crystallizing on a substrate consisting of albite, microcline, quartz, and muscovite-lepidolite micas (Popov

* E-mail: brigatti@unimore.it

and Popova 2006). Our sample is a broken, large, single mica blade (4 cm wide × 0.5 mm thick) that shows a strong color zonation. The zones are 0.4–0.6 cm wide hexagonal bands, changing from light purple to grayish with no visible gradation, with the bands apparently due to numerous very fine inclusions.

In the Sawtooth Mountains (Boise County, Idaho, U.S.A., labeled “Boise”) trioctahedral Li-rich micas may be found in miarolitic cavities of a granite batholith that occurs primarily in Elmore County, where the best collecting is found (Menzies and Boggs 1993). However, this sample is from nearby Boise County, and consists of purple flakes on a substrate of quartz and K-feldspar, with rare anatase.

Electron-microprobe analysis and recalculation of the formula unit

Scanning-electron microscope analyses (Philips SEM XL-40 with an energy dispersive detector), also providing back-scattered electron imaging and X-ray maps, were performed on the samples to determine the cause of possible crystal zoning. All of the following investigations addressed crystals that showed no chemical inhomogeneity after this first check.

Chemical compositions (Table 1) were determined using a wavelength-dispersive ARL-SEM-Q electron microprobe (operating conditions: 15 kV accelerating voltage, 15 nA sample current, and 5 μm beam diameter). Analyses were performed using the Probe software package of Donovan (1995). The following standards were used: microcline (K,Al), albite (Na), spessartine (Mn), ilmenite (Fe,Ti), clinopyroxene (Si,Ca), olivine (Mg), chromite (Cr), pollucite (Cs), fluorite (F), sodalite (Cl), and synthetic Rb-rich glass (Rb). The F content was determined by the method of Foley (1989). No evidence of volatilization of F was observed. Trace elements (wt% oxide < 0.01) are Cs and Cl. Lithium determinations were performed on selected homogeneous portions from the same sample (or sample portion) used in the structure refinement by inductively coupled plasma atomic-emission spectrometry (ICP-AES, Varian Liberty 200). A sample 25 mg in size was digested with a mixture of HF (62%) and HNO₃ (38%) in closed Teflon crucibles in a microwave oven. Chemical formulae (Table 1) are based on O₁₀(F,OH)₂.

X-ray diffraction data

Crystals were mounted on a Bruker X8 APEX four-circle diffractometer combined with a APEX 4K CCD detector, flat graphite monochromator, and MoKα radiation from a fine-focus sealed tube. The SMART software package was used to determine the unit cell and for X-ray data collection (Table 2). Redundant data were collected for an approximate sphere of reciprocal space and were integrated and corrected for background and Lorentz-polarization factors using the Bruker program SAINT+ (Bruker 1999a). The Bruker SADABS (Bruker 1999b) package

was used to apply a semi-empirical absorption correction. The crystal structure was refined using the SHELX-97 package of programs (Sheldrick 1997) in space group C2 with neutral atomic scattering factors, starting from the atomic coordinates of Brigatti et al. (2000). Positional and displacement parameters are reported in Table 3¹. Anisotropic displacement parameters were refined for all atoms. Table 4 lists selected interatomic distances and parameters obtained from structural refinements. The mean-electron counts at M1, M2, M3, and A sites were calculated combining structural model and electron microprobe analysis (Table 1). Table 5 reports the refined and calculated octahedral and interlayer site occupancies. Additional parameters derived from the model refinement are reported in Table 6.

RESULTS AND DISCUSSION

Chemistry

The chemical compositions of our Li-, Fe-, and Mn-rich micas are reported in Table 1 and in Figure 1¹. A general overview and their correct placement in the frameset of Li-rich trioctahedral micas can be gained from the classification diagram (*feal-mgli*) introduced by Tischendorf et al. (2004). Our samples lie in the zinnwaldite field and are close in composition to some samples described by Förster et al. (2005). This classification diagram does not distinguish Mn-micas, so that the Sawtooth Mountains zinnwaldite, with Mn > 0.5 apfu, is actually a masutomilite.

The Fe-Li-Mn diagram indicates that these Li-, Fe-, and Mn-rich micas show solid solutions between Fe-rich polyolithionite and masutomilite (Fig. 2). Based on Rieder et al. (1998) only the

¹ Deposit item AM-07-027, Tables 3, 5, and Figure 1 (chemical compositions of our Li-, Fe-, and Mn-rich micas). Deposit items are available two ways: For a paper copy contact the Business Office of the Mineralogical Society of America (see inside front cover of recent issue) for price information. For an electronic copy visit the MSA web site at <http://www.minsocam.org>, go to the American Mineralogist Contents, find the table of contents for the specific volume/issue wanted, and then click on the deposit link there.

TABLE 1. Chemical data and mean electron counts (m.e.c) for Fe-, Mn-, and Li-rich micas-1M

	Hirukawa	Mokruscha	Boise		Hirukawa	Mokruscha	Boise
		wt%			Unit-cell content based on O ₁₀ (OH,F) ₂		
SiO ₂	47.60	45.34	41.19	²⁸ Si	3.43	3.30	3.11
Al ₂ O ₃	18.60	19.80	20.35	²⁷ Al	0.57	0.70	0.89
TiO ₂	0.03	0.01	0.31	⁴⁶ Sum	4.00	4.00	4.00
Cr ₂ O ₃	0.02	b.d.t.	b.d.t.	²⁷ Al	1.00	1.00	0.91
FeO	6.30	5.94	7.24	⁴⁸ Ti	–	–	0.02
MgO	0.05	0.05	0.28	⁵⁶ Fe ²⁺	0.38	0.36	0.46
MnO	2.83	4.96	8.16	²⁴ Mg	0.01	0.01	0.03
Li ₂ O	4.97	4.51	3.50	⁵⁵ Mn	0.17	0.31	0.52
BaO	0.04	0.03	0.11	⁷ Li	1.44	1.32	1.06
CaO	0.02	0.16	0.05	⁴⁶ Sum	3.00	3.00	3.00
Na ₂ O	0.35	0.30	0.33	⁴⁰ Ca	–	0.01	–
Rb ₂ O	0.04	0.10	0.43	²³ Na	0.05	0.04	0.05
K ₂ O	10.33	10.11	9.61	³⁹ K	0.95	0.94	0.92
F	8.27	8.30	7.93	⁸⁵ Rb	–	0.01	0.02
H ₂ O*	0.50	0.36	0.44	⁴⁸ Sum	1.00	1.00	0.99
Sum	99.95	99.97	99.93	F	1.88	1.91	1.89
				OH	0.12	0.09	0.11
				O	10.00	10.00	10.00
m.e.c. (e ⁻) at octahedral sites							
M1 (Xref)	9.22(7)	10.59(8)	14.04(7)	m.e.c. (e ⁻) at interlayer sites			
M2 (Xref)	13.03(4)	12.98(8)	12.60(6)	A (Xref)	18.69(6)	18.96(7)	19.19(6)
M3(Xref)	9.37(7)	10.49(8)	13.58(6)	A (EPMA)	18.60	18.87	18.77
M1+M2+M3 (Xref)	31.62	33.07	40.22				
M1+M2+M3 (EPMA)	31.57	34.19	40.77				

Notes: Estimated standard deviations in parenthesis for this and subsequent tables. b.d.t. = below detection threshold. Xref = X-ray diffraction structure refinement; EPMA = electron microprobe analysis.

* Calculated.

TABLE 2. Details on the data collection and structure refinement of Fe-, Mn-, and Li-rich lithian-1M crystals in space group C2

Samples	Crystal dimensions (mm)	Range 2θ (°)	N	R_{obs} ×100	Unit-cell parameters				
					a (Å)	b (Å)	c (Å)	β (°)	V (Å ³)
Hirukawa	0.07 × 0.08 × 0.02	4.1–27.6	1041	3.86	5.264(1)	9.086(2)	10.099(3)	100.719(5)	474.6(2)
Mokrusha	0.04 × 0.06 × 0.02	4.1–29.9	873	3.98	5.297(5)	9.133(7)	10.168(9)	100.78(2)	483.2(7)
Boise	0.10 × 0.8 × 0.02	4.1–33.7	1721	3.98	5.2984(3)	9.1461(6)	10.0966(7)	100.818(4)	480.58(5)

Note: N = number of unique reflections; R_{obs} = structure refinement agreement factor.

TABLE 4. Bond distances (Å) for Fe-, Mn-, and Li-rich micas-1M [space group C2; layer symmetry C121(1)]

Hirukawa			Mokrusha			Boise					
Tetrahedron (T1)			Octahedron (M1)			Interlayer cation					
T1-O1	1.626(7)	1.633(7)	1.630(4)	M1-O3 (×2)	2.141(9)	2.166(9)	2.145(4)	A-O1 (×2)	3.041(3)	3.016(4)	3.037(2)
T1-O2	1.641(6)	1.654(7)	1.648(3)	M1-O33 (×2)	2.123(8)	2.113(8)	2.138(4)	A-O1' (×2)	3.223(3)	3.297(4)	3.265(2)
T1-O22	1.611(7)	1.640(7)	1.647(3)	M1-O4 (×2)	2.130(7)	2.123(7)	2.141(4)	A-O2 (×2)	3.039(6)	2.994(6)	3.037(3)
T1-O3	1.621(7)	1.642(7)	1.640(4)	<M1-O>	2.131	2.134	2.141	A-O2' (×2)	3.194(7)	3.252(7)	3.259(4)
<T1-O>	1.625	1.642	1.641	Octahedron (M2)			A-O22 (×2)	3.011(6)	3.023(6)	3.003(3)	
Tetrahedron (T11)			Octahedron (M2)			A-O22' (×2)			3.153(7)	3.213(7)	3.157(4)
T11-O1	1.652(7)	1.661(7)	1.654(4)	M2-O3 (×2)	1.901(8)	1.897(8)	1.902(4)	<A-O> _{inner}	3.030	3.011	3.026
T11-O2	1.661(7)	1.671(7)	1.638(3)	M2-O33 (×2)	1.903(6)	1.922(6)	1.905(3)	<A-O> _{outer}	3.190	3.254	3.227
T11-O22	1.647(7)	1.642(6)	1.639(3)	M2-O4 (×2)	1.845(6)	1.882(5)	1.864(3)				
T11-O33	1.622(7)	1.641(7)	1.639(4)	<M2-O>	1.883	1.900	1.890				
<T11-O>	1.646	1.654	1.643	Octahedron (M3)							
			M3-O3 (×2)			2.109(6)	2.102(6)	2.130(3)			
			M3-O33 (×2)			2.123(9)	2.137(9)	2.144(4)			
			M3-O4 (×2)			2.137(8)	2.127(6)	2.153(3)			
			<M3-O>			2.123	2.122	2.142			

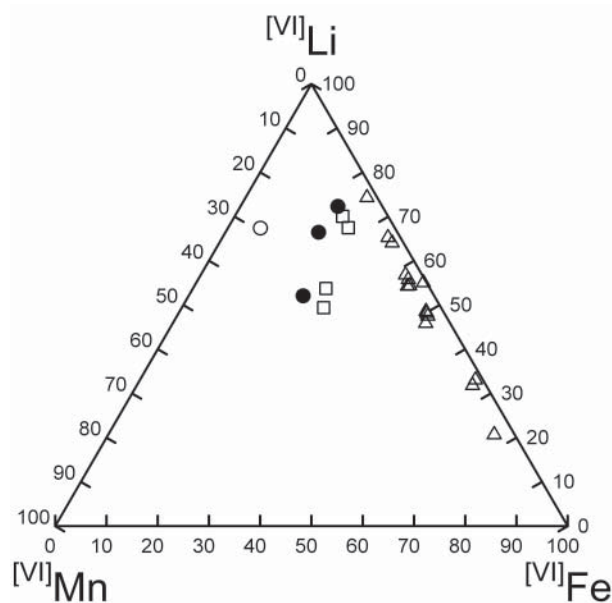


FIGURE 2. Ternary $^{VI}\text{Fe}-^{VI}\text{Li}-^{VI}\text{Mn}$ diagram showing compositional data of Li-, Fe-, and Mn-rich micas. Symbols: filled circle = this study; open circle = Mizota et al. 1986; open squares = Förster et al. 2005; open triangles = Brigatti et al. 2000.

sample from Boise is masutomilite; all the others are intermediate solid solutions showing greater Fe than Mn content. Note also that Li and Si content decreases with increasing Mn content.

All samples are rich in F. According to Černý et al. (1985, 1986), the F content in octahedral sites is strictly associated with Mn, in samples where Mn for Fe substitution occurs.

Crystal structure

One of the relevant features for the Li-, Fe-, and Mn-rich micas studied is the difference in size and scattering efficiency

TABLE 6. Selected parameters derived from structure refinement for Fe-, Mn-, and Li-rich mica crystals

	Hirukawa	Mokrusha	Boise
Tetrahedral parameters			
α (°)	3.6(1)	5.4(2)	4.4(1)
Δz (Å)	0.0824	0.0839	0.1289
τ _{T1} (°)	112.0(1)	111.9(2)	111.1(1)
τ _{T11} (°)	112.0(2)	111.6(3)	111.1(1)
Tetrahedral basal area T1 (Å ²)	2.952	3.015	3.046
Tetrahedral basal area T11 (Å ²)	3.053	3.089	3.057
Octahedral parameters			
ψ _{M1} (°)	60.660.8	60.6	
ψ _{M2} (°)	56.356.7	56.2	
ψ _{M3} (°)	60.560.6	60.6	
O3-O3 _{M1}	3.180(3)	3.187(5)	3.196(2)
O3-O3 _{M2}	2.764(4)	2.803(6)	2.759(3)
O3-O3 _{M3}	3.176(3)	3.179(4)	3.228(2)
O3-O4 _{M1}	3.268(3)	3.277(5)	3.269(2)
O3-O4 _{M2}	3.203(3)	3.211(4)	3.234(2)
O3-O4 _{M3}	2.686(4)	2.722(6)	2.712(3)
O3-O4 _{M2}	2.687(4)	2.727(5)	2.695(3)
O3-O4 _{M3}	3.177(3)	3.181(4)	3.208(2)
O3-O4 _{M3}	3.243(3)	3.244(4)	3.265(2)
Out of center shift along [010], M1 (Å)	0.0127	0.0143	0.0058
Out of center shift along [010], M2 (Å)	0.0130	0.0393	0.0155
Out of center shift along [010], M3 (Å)	0.0285	0.0161	0.0308
Layer thickness			
Tetrahedral	2.252	2.271	2.244
Octahedral	2.092	2.085	2.100
Interlayer	3.327	3.361	3.330

between the octahedral M2 and M3 sites (Tables 1 and 4), which accounts for the reduction from C2/m to C2 in symmetry [or from C12/m1(1) to C121(1), referring to diperic groups]. Thus, three different cation sites occur in the octahedral sheet: M1, M2, and M3. For all studied crystals, the M1 (2.131 ≤ <M1-O> ≤ 2.141 Å) and M3 (2.122 ≤ <M3-O> ≤ 2.142 Å) sites are much greater in size than M2 (1.883 ≤ <M2-O> ≤ 1.900 Å). The differences in mean bond length between the M2 and M3 sites (Δ<M-O>_{M2,M3}) vary from 0.222 to 0.252. The greatest difference was observed for the Boise sample, characterized by the high-

est Mn, Fe, and Ti contents. The resulting mean bond distances (Table 4) together with the scattering efficiencies (Table 1) for the M1, M2, and M3 sites indicate meso-octahedral ordering (Đurovič et al. 1984; Đurovič 1994), which is also confirmed by the determined mean electron counts, where m.e.c. $M1 \approx$ m.e.c. $M3 <$ m.e.c. $M2$ for the Hirukawa and Mokrusha samples and m.e.c. $M1 \approx$ m.e.c. $M3 >$ m.e.c. $M2$ for the Boise sample. The mean electron counts determined for the M2 sites show limited variation ($12.60 \leq$ m.e.c. $M2 \leq 13.03$), unlike M1 ($9.22 \leq$ m.e.c. $M1 \leq 14.04$) and M3 ($9.37 \leq$ m.e.c. $M3 \leq 13.58$). Thus, based on mean electron counts, mean bond distances and chemical analyses, we conclude that Al preferentially occupies the M2 site, whereas Mn (and/or Fe) and Li are disordered between M1 and M3 sites (Table 5¹).

The hexagon defined by the O3-O3 octahedral edges i.e., the “octahedral hexagon,” as defined by Brigatti et al. (2003), is highly distorted (Fig. 3a, Table 6). The greatest difference in length between the O3-O33 edge for M3 (O3_F-O33_A), which is the largest edge, and that for M2 (O3_D-O33_E) occurs in the Boise sample at 0.469 Å. This structural feature is a result of the different octahedral sizes produced by the cation ordering

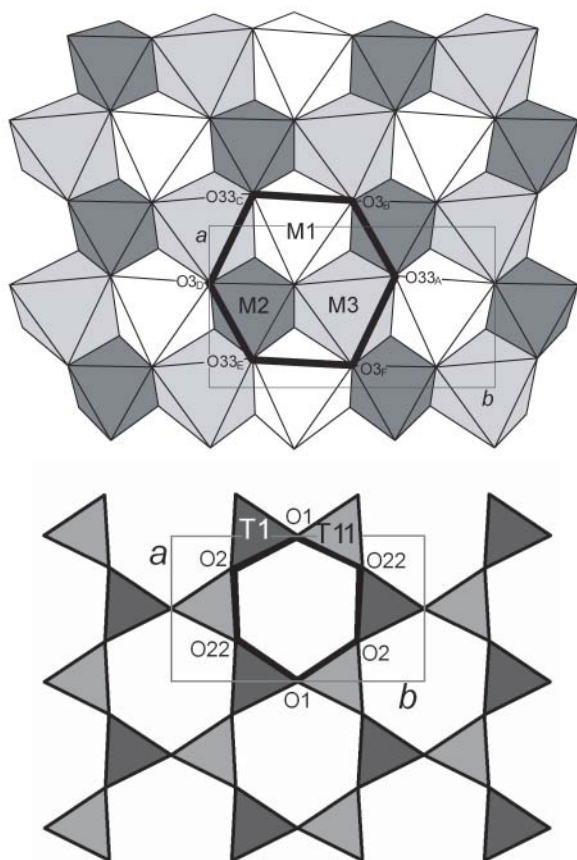


FIGURE 3. (a) M1, M2, and M3 site arrangement projected on (001). Bold lines define the octahedral hexagon ring outlined by O3 and O33 oxygen atoms. Labels A to F are introduced to identify each oxygen atom in the octahedral hexagon ring. (b) T1 and T11 site arrangement projected on (001). Bold line defines the tetrahedral hexagon ring outlined by O1, O2, and O22 oxygen atoms.

in the *cis* octahedral sites.

Tetrahedral mean bond lengths are apparently smaller for T1 ($1.625 \leq \langle T1-O \rangle \leq 1.642$ Å) than for T11 ($1.643 \leq \langle T11-O \rangle \leq 1.654$ Å), with the greatest difference for the Hirukawa sample at 0.021 Å (standard deviation of the mean value, $\sigma_n = 0.006$ Å). However, the tetrahedral bond distances are equal in the Boise sample (T1 = 1.641 Å; T11 = 1.643 Å). Ordering of tetrahedral cations is favored when small, high-charged cations are ordered in the octahedral sites (Guggenheim 1984), and it is rare in true micas (Brigatti and Guggenheim 2002). The Li-, Fe-, and Mn-rich micas have one octahedral smaller and two larger octahedral sites: the latter sites probably host lower-charge cations (i.e., Fe²⁺, Mn²⁺, and Li⁺), whereas the former is probably occupied by higher-charge cations (i.e., Al³⁺). In the samples considered, the greatest difference in mean electron count for octahedral sites is observed in the Hirukawa sample, which also shows a significant tetrahedral ordering. On the contrary, the minimum variation is observed in the Boise sample, which shows no ordering at all. Our data thus seem to support the observation reported by Guggenheim (1984).

Both the T1 and T11 tetrahedra are elongated with τ angle values varying from 111.1 to 112.0°, which are greater than the ideal 109.47° value. The tetrahedral basal area is greater for T11 (varying from 3.053 to 3.089 Å²) than for T1 (varying from 2.952 to 3.046 Å²). Tetrahedral rotation angle α varies from 3.6 to 5.4° (Table 6). The lowest value was found in the Hirukawa sample, characterized by the lowest Fe and Mn contents, whereas the highest tetrahedral rotation was found in the Boise sample, which shows the highest Mn + Fe_{total} content. This latter trend is unusual. In trioctahedral true micas, an increase in Fe substitution enlarges the octahedral sheet, thus favoring a match with the tetrahedral sheet that requires a lower α value. An explanation for this feature is suggested in the crystal chemistry section.

Although the limited number of samples studied prevents a definitive conclusion, Mn content in Li-rich micas affects the T11 tetrahedral dimensions and distortion, in particular the τ angle (Table 6); based on this limited set of data, the preferential segregation of tetrahedral Al in T11 follows the exchange vector: ${}^VI\text{Li}_{-1}{}^{IV}\text{Si}_{-1}{}^{VI}\text{Mn}{}^{IV}\text{Al}$.

Crystal chemistry

As shown by Förster et al. (2005), and also confirmed by our samples, substantial Fe and Mn can substitute for Al and Li in the octahedral sites of Li-rich trioctahedral micas (Fig. 4a). However, Li is favored over Al, thus leading to a reduction in octahedral charge when substituting Fe and/or Mn (Fig. 4b).

The present data set, which includes previously studied Li- and Fe-rich micas (Brigatti et al. 2000), masutomilite (Mizota et al. 1986), and our three Li-, Fe-, and Mn-rich micas follow similar crystal chemical trends. These trends suggest similar roles for Fe and Mn octahedral cations. The increasing octahedral charge, which is correlated with the variation in the Fe and/or Mn substitution, is charge-balanced both via anionic oxy-substitutions, in Li- and Fe-rich samples, and via the substitution of Si in the tetrahedral sites, as previously discussed. This latter exchange mechanism defines the join connecting polyolithionite to siderophyllite.

One important crystallochemical effect involves the overall

layer dimensions, which increase when Fe and/or Mn substitution for Al and Li occurs (Fig. 5a). The variation in lateral unit-cell parameters, which is directly related to octahedral sheet dimensions (Brigatti and Guggenheim 2002), induces a similar variation in tetrahedral basal distances. Thus, a topological matching of octahedral and tetrahedral sheets (Fig. 5b) must occur. Therefore, mean tetrahedral basal edges, mean octahedral hexagon edge and mean O3-O4 octahedral distances increase together with the Mn + Fe_{total} content. Similar trends can also be defined for the octahedral hexagon area, defined by tetrahedral apical oxygen atoms (Fig. 2a), and for the tetrahedral hexagon area, defined by basal tetrahedral oxygen atoms (Fig. 2b).

Alternatively, dimensional matching between the octahedral and tetrahedral sheets could be achieved via a variation in the tetrahedral rotation angle (α). However, this is not the case for Li-, Fe-, and Mn-rich micas, as the α angle is not significantly affected by chemical composition, varying in a restricted range from 3.6–5.4°. This behavior is probably explained by the concomitant increase in the Al tetrahedral content, which increases with Fe and/or Mn substitution, thus producing an expansion of both the tetrahedral and octahedral sheets. An associated effect is also observed in the tetrahedral volume, which increases with Fe and/or Mn substitution. This substitution also causes a reduction of the tetrahedral flattening angle τ , which reflects an enlargement of the basal tetrahedral area and an increased tetrahedral Al content (Brigatti and Guggenheim 2002).

As discussed above, M2 and M3 are very different in size and the latter is close in size to M1. The size of the smaller octahedral

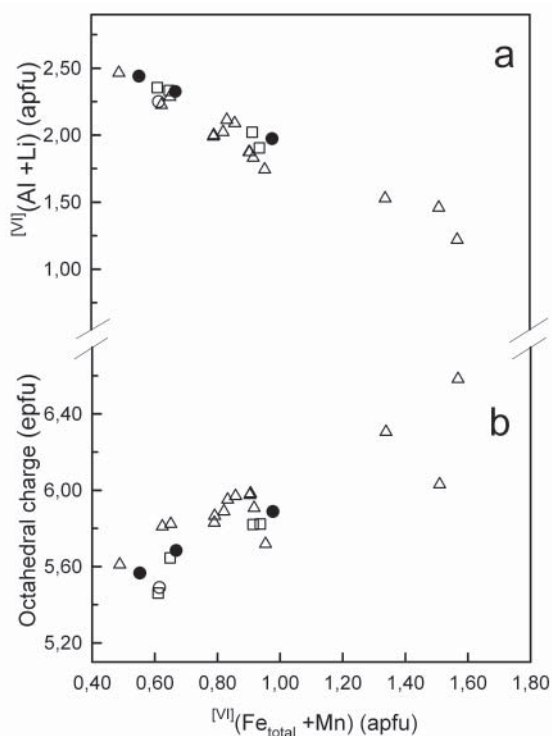


FIGURE 4. Variation of (a) VI(Al + Li) (apfu) and (b) octahedral sheet charge with VI(Fe_{total} + Mn) (apfu). Symbols and samples as in Figure 2.

site seems to increase with Ti content based on our limited data set. Even if present in limited amount, Ti can play a significant role in determining the value of many octahedral parameters, especially those involving the anionic O4 site that may include F substitution. Thus the A-O4 distance along (001) decreases with increasing Ti, whereas the O4-O4 octahedral edge, shared between M2 and M3, increases (Fig. 6).

The dimensions of the two large octahedral sites appear to be affected by tetrahedral composition and they increase in size with

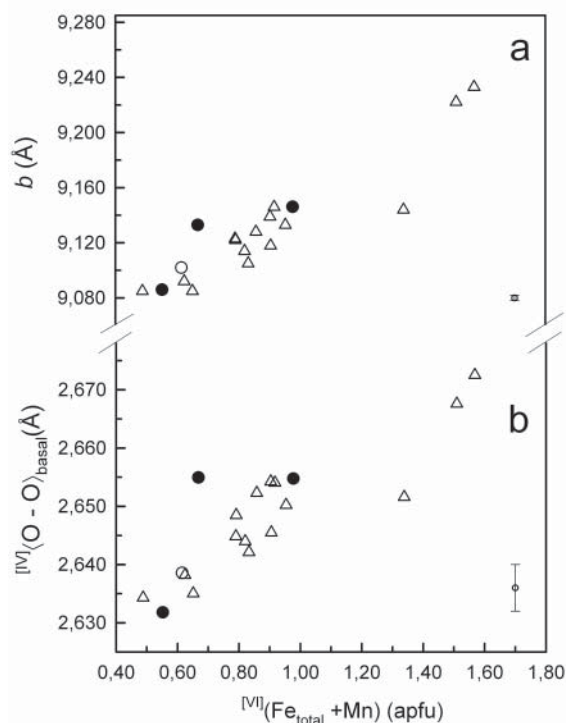


FIGURE 5. Compositional dependence of (a) unit-cell parameter *b* (Å) and (b) of mean tetrahedral basal edge IV(O-O)_{basal} (Å) with VI(Fe_{total} + Mn) (apfu). Symbols: filled circle = this study; open circle = Mizota et al. 1986; open triangles = Brigatti et al. 2000. Estimated mean error bar is given in the lower-right corner of each graph.

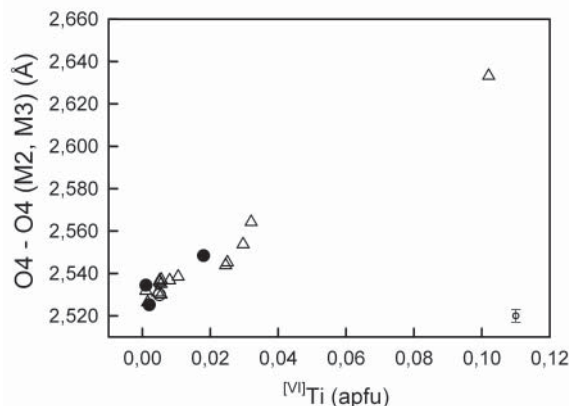


FIGURE 6. Variation of the O4-O4 (Å) octahedral edge shared between M2 and M3 as a function of the octahedral Ti content. Estimated mean error bar is given in the lower-right corner.

tetrahedral Al content, probably reflecting the overall constraints as required from the dimensional matching of the tetrahedral and octahedral sheets.

ACKNOWLEDGMENTS

The comments from W.C. Elliot, S. Guggenheim, and M. Mellini significantly contributed to the improvement of this work. Ing. Renato Pagano kindly supplied the examined samples. This work was made possible by the financial support of Ministero dell'Università e della Ricerca Scientifica of Italy (MIUR PRIN2006).

REFERENCES CITED

- Abdalla, H.M., Ishihara, S., Matsueda, H., and Abdel Monem, A.A. (1996) On the albite-enriched granitoids at Um Ara area, Southeastern Desert, Egypt. 1. Geochemical, ore potentiality and fluid inclusion studies. *Journal of Geochemical Exploration*, 57, 127–138.
- Backhaus, K.O. (1983) Structure refinement of a lepidolite-1M. *Crystal Research Technology*, 18, 1253–1260.
- Brigatti, M.F. and Guggenheim, S. (2002) Mica crystal chemistry and the influence of pressure, temperature, and solid solution on atomistic models. In A. Motana, F.P. Sassi, J.B. Thompson Jr., and S. Guggenheim, Eds., *Micas: crystal chemistry and metamorphic petrology*, 46, p. 1–97. Reviews in Mineralogy and Geochemistry, Mineralogical Society of America, Chantilly, Virginia.
- Brigatti, M.F., Lugli, C., Poppi, L., Foord, E.E., and Kile, D.E. (2000) Crystal chemical variations in Li- and Fe-rich micas from the Pikes Peak batholith (central Colorado). *American Mineralogist*, 85, 1275–1286.
- Brigatti, M.F., Guggenheim, S., and Poppi, M. (2003) Crystal chemistry of the 1M mica polytype: The octahedral sheet. *American Mineralogist*, 88, 667–675.
- Bruker AXS (1999a) SAINT+ (version 6.01). Bruker AXS Inc., Madison, Wisconsin.
- (1999b) SADABS (version 2.03). Bruker/Siemens area detector absorption and other corrections. Bruker AXS Inc, Madison, Wisconsin.
- Černý, P., Meintzer, R.E., and Anderson, A.J. (1985) Extreme fractionation in rare-element granitic pegmatites: selected examples of data and mechanisms. *Canadian Mineralogist*, 23, 381–421.
- Černý, P., Goad, B.E., Hawthorne, F.C., and Chapman, R. (1986) Fractionation trends of the niobium- and tantalum-bearing oxide minerals in the Greer Lake pegmatitic granite and its pegmatite aureole, southeastern Manitoba. *American Mineralogist*, 71, 501–517.
- Donovan, J.J. (1995) PROBE: PC-based data acquisition and processing for electron microprobes. Advanced Microbeam, Vienna, Ohio.
- Dornberger-Schiff, K., Backhaus, K.O., and Đurovič, S. (1982) Polytypism of micas: OD-interpretation, stacking symbols, symmetry relations. *Clays and Clay Minerals*, 30, 364–374.
- Đurovič, S. (1994) Classification of phyllosilicates according to the symmetry of their octahedral sheet. *Silikáty*, 38, 81–84.
- Đurovič, S., Weiss, Z., and Backhaus, K.O. (1984) Polytypism of micas. II Classification and abundance of MDO polytypes. *Clays and Clay Minerals*, 32, 464–474.
- Eggleton, R.A. and Ashley, P.M. (1989) Norrishite, a new manganese mica, $K(\text{Mn}^{2+}\text{Li})\text{Si}_4\text{O}_{12}$, from the Hoskins mine, New South Wales, Australia. *American Mineralogist*, 74, 1360–1367.
- Foley, S.F. (1989) Experimental constraints on phlogopite chemistry in lamproites: 1. The effect of water activity and oxygen fugacity. *European Journal of Mineralogy*, 1, 411–426.
- Förster, H.-J., Tischendorf, G., Rhede, D., Naumann, R., Gottesmann, B., and Lange, W. (2005) Cs-rich lithium micas and Mn-rich lithian siderophyllite in miarolitic NYF pegmatites of the Koenigshain granite, Lausitz, Germany. *Neues Jahrbuch für Mineralogie, Abhandlungen*, 182, 81–93.
- Guggenheim, S. (1981) Cation ordering in lepidolite. *American Mineralogist*, 66, 1221–1232.
- (1984) The brittle micas. In S.W. Bailey, Ed., *Micas*, 13, p. 61–104. Reviews in Mineralogy, Mineralogical Society of America, Chantilly, Virginia.
- Guggenheim, S. and Bailey, S.W. (1977) The refinement of zinnwaldite-1M in subgroup symmetry. *American Mineralogist*, 62, 1158–1167.
- Harada, K., Honda, M., Nagashima, K., and Kanisawa, S. (1976) Masutomilite, manganese analog of zinnwaldite, with special reference to masutomilite-lepidolite-zinnwaldite series. *Mineralogical Journal (Japan)*, 8, 95–109.
- Menzies, M.A. and Boggs, R.C. (1993) Minerals of the Sawtooth Batholith, Idaho. *Mineralogical Record*, 24, 185–202.
- Mizota, T., Kato, T., and Harada, K. (1986) The crystal structure of masutomilite, manganese analog of zinnwaldite. *Mineralogical Journal (Japan)*, 13, 13–21.
- Němec, D. (1983a) Masutomilite in lithium pegmatites of West-Moravia, Czechoslovakia. *Neues Jahrbuch für Mineralogie, Monatshefte*, 1983, 537–540.
- (1983b) Zinnwaldite in Moldanubian lithium pegmatites. *Chemie der Erde*, 42, 197–204.
- Popov, V.A. and Popova, V.I. (2006) Ilmeny Mountains (Russia): Mineralogy of Pegmatites. In I.V. Pekov, Ed., *Mineralogical Almanac*, 9, 156 p. Institute of Mineralogy of Ural Branch RAS, Lomonosov Moscow State University, Russian Geological Society.
- Rieder, M., Cavazzini, G., D'yakonov, Y.S., Frank-Kamenetskii, V.A., Gottardi, G., Guggenheim, S., Koval, P.V., Müller, G., Neiva, A.M.R., Radoslovich, E.W., Robert, J.-L., Sassi, F.P., Takeda, H., Weiss, Z., and Wones, D.R. (1998) Nomenclature of the micas. *Clays and Clay Minerals*, 41, 61–72.
- Sheldrick, G.M. (1997) SHELX-97, program for crystal structure determination. University of Göttingen, Germany.
- Sueno, S., Matsura, S., Bunno, M., and Kurosawa, M. (2002) Occurrence and crystal chemical features of protoferro-anthophyllite and protomangano-ferroanthophyllite from Cheyenne Canyon and Cheyenne Mountain, U.S.A. and Hirukawa-mura, Suisho-yama, and Yokone-yama, Japan. *Journal of Mineralogical and Petrological Sciences*, 97, 127–136.
- Tischendorf, G., Rieder, M., Foerster, H.-J., Gottesmann, B., and Guidotti, C.V. (2004) A new graphical presentation and subdivision of potassium micas. *Mineralogical Magazine*, 68, 649–667.
- Tyrna, P.L. and Guggenheim, S. (1991) The crystal structure of norrishite, $\text{KLiMn}^{2+}\text{Si}_4\text{O}_{12}$: an oxygen-rich mica. *American Mineralogist*, 76, 266–271.

MANUSCRIPT RECEIVED NOVEMBER 2, 2006

MANUSCRIPT ACCEPTED APRIL 26, 2007

MANUSCRIPT HAND LED BY W. CRAWFORD ELLIOTT